The Company of Biologists

RESEARCH ARTICLE

F-actin flashes on phagosomes mechanically deform contents for efficient digestion in macrophages

Mathieu B. Poirier, Cara Fiorino, Thiviya K. Rajasekar and Rene E. Harrison*

ABSTRACT

The mechanism and role of transient F-actin recruitment, or F-actin 'flashes', on phagosomes remains enigmatic. Here we provide a comprehensive characterization of F-actin flashing dynamics on phagosomes, including receptor and signaling involvement. F-actin flashes predominate during the integrin-driven complement receptor (CR)-mediated phagocytosis. F-actin flashes begin shortly after internalization and persist on phagosomes for approximately 3 minutes before disassembling and reassembling several times within the first hour. Strikingly, the appearance of F-actin flashes on phagosomes coincides with morphological deformation, lysis and occasional fission of internalized red blood cells. The cadence of flashes depends on particle stiffness, and the F-actin networks on phagosomes are enriched in mechanosensitive components including focal adhesion proteins, RhoA and actomyosin. Inhibiting Arp2/3 and myosin IIA activity significantly reduces the frequency at which phagosome cargo becomes deformed during transient F-actin accumulation. At later time points, post-F-actin flashing, enhanced degradation of phagosome contents is observed, compared with non-flashing phagosomes. Taken together, these data suggest that actomyosin-driven phagosome contractions serve to disrupt malleable particles physically, a process akin to mastication, to enhance later enzymatic digestion.

KEY WORDS: Macrophages, Phagocytosis, Complement, Phagosome maturation

INTRODUCTION

Phagocytosis is the uptake process of relatively large target particles by specialized innate immune cells and amoeba. Phagocytosis in macrophages is characterized by dramatic F-actin protrusions that are orchestrated by opsonic receptor signaling. The major opsonic receptors in macrophages are Fcγ receptors that recognize bound IgG and complement receptor 3 (CR3) that binds to deposited complement protein fragment C3bi on target particles. Studies so far have revealed striking differences between the modes of phagocytosis induced by the opsonic receptors in macrophages, including a strong requirement for the RhoA GTPase, but not Rac1 and Cdc42, for CR-mediated phagocytosis (Caron and Hall, 1998). Our laboratory has chosen to delve into the poorly understood CR-mediated phagocytosis and shown that membrane ruffles actively capture C3bi-opsonized targets (Patel and Harrison,

2008), challenging the previous dogma that C3bi particles passively sink into the cell. Once internalized, the subsequent process of phagosome maturation is better understood for FcγR-mediated phagocytosis in macrophages. During engulfment of IgG-coated particles, F-actin disassembly occurs around the phagosome to facilitate interactions with the endocytic pathway, which drives content acidification and degradation.

Although F-actin is believed to be an impediment to phagosome maturation, the presence of transient accumulations of F-actin on phagosomes has been observed during uptake of bacteria and IgG-opsonized particles. These 'F-actin flashes' were first described in Madin–Darby canine kidney (MDCK) epithelial cell phagosomes containing *Listeria monocytogenes* (Yam and Theriot, 2004). Manipulation of bacteria surface and effector proteins determined that this was a host cell-driven event. F-actin flashes were also observed in macrophages overloaded with IgG-opsonized latex beads (Liebl and Griffiths, 2009). Macrophages with increased phagocytic load had a greater incidence of F-actin flashing, effectively reducing the rate of maturation (as shown by lowered LAMP2 recruitment to phagosomes). In addition, the authors determined that phagosome membrane curvatures presented a surface that was favorable for actin nucleation (Liebl and Griffiths, 2009). Other observed F-actin accumulations on phagosomes included F-actin comet tails on CR-phagosomes in macrophages that could potentially propel phagosomes towards lysosomes (Bohdanowicz et al., 2010).

In this investigation, we have focused on the mechanism and function of F-actin flashes on phagosomes. F-actin flashes transiently encompass the phagosome and are cyclical in nature over the first hour of internalization. F-actin flashes predominate on integrin-based CR-phagosomes and involve recruitment of focal adhesion proteins and RhoA signaling. Interestingly, the rigidity of the phagosome contents influences F-actin flashing dynamics on phagosomes. F-actin flashes show strong myosin II recruitment, and myosin II activity drives phagosome content deformation. Interestingly, phagosomes that exhibit F-actin flashes show accelerated degradation at later time points. Thus, we have evidence showing for the first time that an active 'chewing' mechanism may be at play during intracellular particle destruction in macrophages.

RESULTS

F-actin flashes are prominent during CR-mediated phagocytosis and are associated with particle deformation

Our laboratory studies CR-mediated phagocytosis and we have previously shown a prominent role for F-actin in mediating membrane ruffle capture of C3bi-opsonized targets. To image F-actin, we generated RAW 264.7 cells stably transfected with fluorescent LifeAct (RAW-LifeAct) constructs (Riedl et al., 2008). Transfected cells were treated with phorbol myristate acetate (PMA) to activate CR (Wright and Silverstein, 1982), exposed to

C3bi-opsonized sheep red blood cells (sRBCs) and imaged with epifluorescence microscopy. We saw the characteristic F-actin cup at the time of particle capture, after which the LifeAct-CFP signal dissipated when the sRBC was internalized (Fig. 1A), as expected (Vieira et al., 2002). However, to our surprise, a strong F-actin signal was recruited to the internalized phagosome, which then disappeared and reappeared multiple times over the first hour of particle internalization and finally subsided (Fig. 1A–C; Movie 1). To better visualize the dynamics of the cyclical accumulations of F-actin on CR-phagosomes, we measured LifeAct-CFP signal intensity over time on the phagosome membrane (Fig. 1B). These F-actin flashes were also observed in mouse bone marrow-derived macrophages (BMDMs) transiently transfected with LifeAct-RFP (Fig. 1C). The recurrent phagosome recruitment of F-actin was very reminiscent of F-actin flashes described around internalized *Listeria* in epithelial cells and in macrophages after uptake of IgG-opsonized

latex beads (Liebl and Griffiths, 2009; Yam and Theriot, 2004). We fed RAW-LifeAct cells with IgG-sRBCs to compare the frequency of F-actin flashes between IgG- versus C3bi-opsonized targets. The F-actin flashes were specific to C3bi-opsonized targets, where approximately one-third of phagosomes exhibited flashing, versus IgG-sRBCs which showed less than 5% frequency (Fig. 1D), as reported for IgG-particle-overloaded macrophages (Liebl and Griffiths, 2009). During imaging, we also occasionally observed asymmetric F-actin comet tails on phagosomes that typically appeared once on a phagosome and resulted in particle translocation, as described previously (Bohdanowicz et al., 2010). We quantified these distinct events, which we determined to be rarer than F-actin flashes on CR-phagosomes (Fig. 1E). We next investigated F-actin recruitment to complement-opsonized *Escherichia coli* compartments in macrophages, given that F-actin flashing was observed on internalized bacteria in epithelial cells
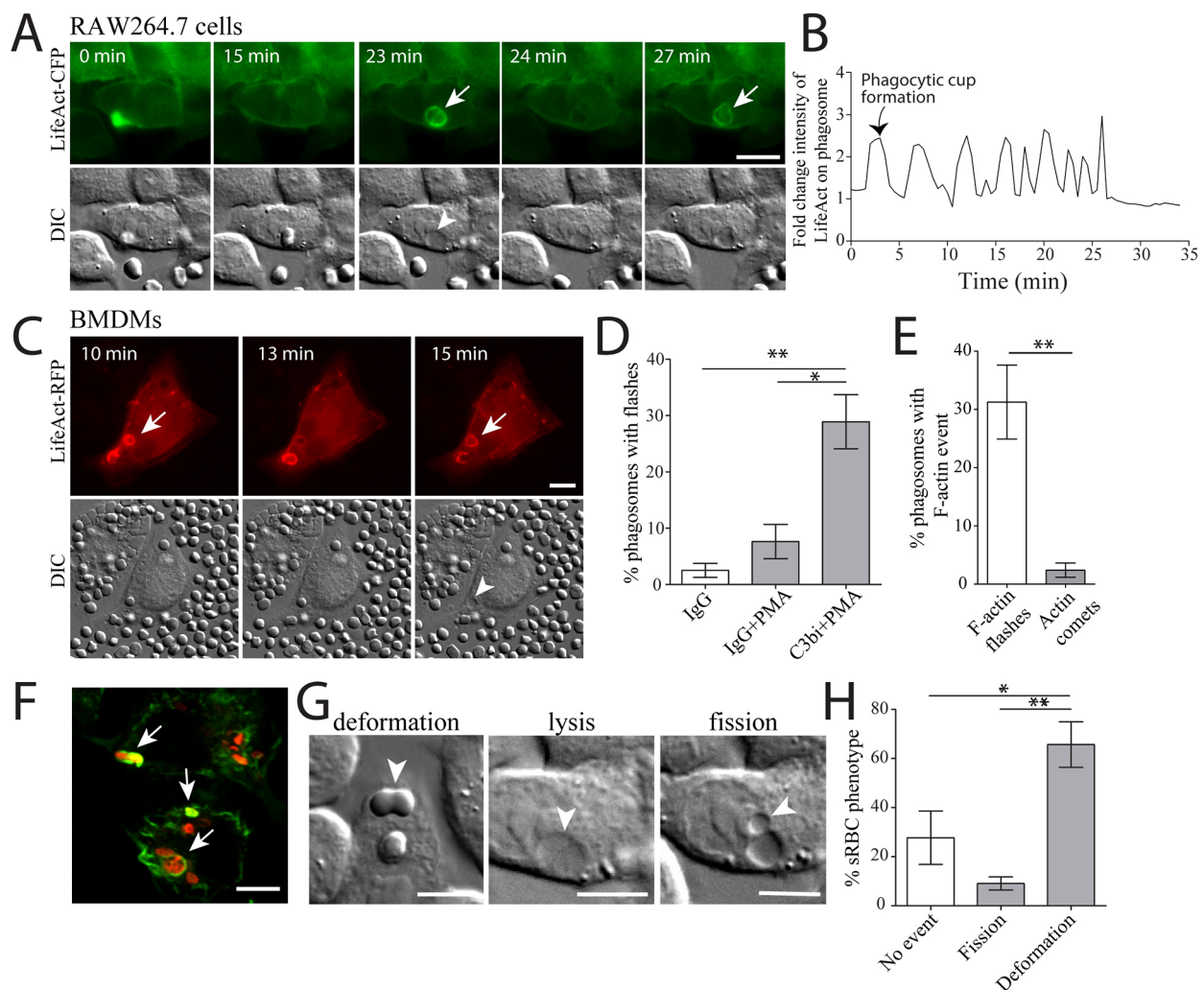

Fig. 1. F-actin flashes occur on CR-phagosomes in macrophages and correlate with particle deformation. (A) Live-cell imaging of RAW 264.7 cells or (C) BMDM cells transfected with LifeAct-CFP or LifeAct-RFP and challenged with C3bi-sRBCs to induce CR-mediated phagocytosis. (B) Line scan showing another typical F-actin flashing event shown as fold change of LifeAct-CFP signal intensity over time (normalized to background) at the CR-phagosome membrane post particle internalization. (D) The frequency of phagosomes exhibiting F-actin flashes was measured in RAW 264.7 cells expressing LifeAct-CFP after ingestion of IgG-sRBCs versus C3bi-sRBCs. PMA was used to activate integrins. (E) The frequency of F-actin flashes on phagosomes versus actin comet tails was also tabulated in RAW 264.7 cells expressing LifeAct-CFP and ingesting C3bi-sRBCs. (F) Immunofluorescence image of RAW 264.7 cells after 40 min of uptake of C3bi-*E. coli* stained with anti-*E. coli* antibodies (red) and phalloidin (green). (G) DIC imaging was performed to assay the fate of sRBCs inside flashing phagosomes. DIC images showing C3bi-sRBC deformation, including cell lysis, as well as some fission events. (H) Quantification of the frequency of these events in flashing phagosomes. For quantifications, $n=50$ phagosomes were assayed in three biological replicates. Error bars represent s.e.m. *$P<0.05$, **$P<0.01$. Arrows indicate F-actin flashes and arrowheads show sRBC lysis in the DIC channel. Scale bars: 10 μm.

(Yam and Theriot, 2004). We saw a strong accumulation of F-actin around internalized C3bi-*E. coli* 40 min after internalization (Fig. 1F).

Our DIC analysis revealed a striking fate of the sRBCs within the F-actin flashing phagosomes (Fig. 1A,C,G; Movie 1). The appearance of F-actin on phagosomes resulted in near-instant sRBC deformation, with fission events and sRBC lysis often occurring (Fig. 1A,C,G,H; Movie 1). These data strongly indicated that the presence of F-actin on phagosomes was mechanically altering the cargo. sRBC integrity was rarely altered in non-flashing phagosomes, showing a strong connection between the appearance of F-actin flashes and cargo manipulation.

Particle rigidity impacts F-actin flashing dynamics on phagosomes

We observed that particle deformation often occurred simultaneously with F-actin recruitment on CR-phagosomes and we hypothesized that phagosome membrane proteins may have mechanosensing properties that detect an engulfed particle's stiffness. We predicted that a disparity between opsonized particles of varying malleability would manifest in the form of changes in the temporal dynamics of F-actin flashes. We compared F-actin flashes on phagosomes containing similarly sized C3bi-sRBCs versus C3bi-beads to represent malleable and rigid particles, respectively. F-actin flashes on phagosomes were monitored using live-cell epifluorescence imaging of RAW 264.7 cells stably transfected with LifeAct-RFP.

The time taken for a single F-actin flash on a phagosome was ~3 min for both opsonized sRBCs and beads (Fig. 2A). The total period of F-actin flashing events was also similar between C3bi-sRBCs and C3bi-beads, ranging at approximately 30 min for both (Fig. 2B). Interestingly, the relative rigidity of the target particle influenced the frequency dynamics of F-actin flashes on phagosomes. Despite each F-actin flash and total duration of all flashes being similar (Fig. 2A,B), the more malleable opsonized particles (sRBCs) had much shorter time intervals between F-actin flashes on phagosomes (Fig. 2C), which resulted in twice as many flashes over the first hour compared with opsonized rigid latex beads (about six versus three, respectively; Fig. 2D). The time from F-actin cup formation until the first F-actin flash on phagosomes was also compared. Phagosomes containing malleable C3bi-sRBCs took ~9 min to flash, whereas the phagosomes containing stiff C3bi-beads showed flashes within ~3.5 min (Fig. 2E); however, this difference was not significant. Interestingly, the prevalence of F-actin flashes was lower on phagosomes with C3bi-beads (13.2±0.6%) compared with phagosomes containing C3bi-sRBCs (36.3±5.7%) (Fig. 2F). Together, the results show that C3bi-sRBCs triggered more instances of F-actin flashes on phagosomes, each having more F-actin recruitment events than phagosomes containing latex beads. A comparative summary of the differential dynamics of F-actin flashes on phagosomes containing C3bi-sRBCs versus C3bi-beads is shown in Fig. 2G,H.

CR3, talin and focal adhesion proteins are recruited to F-actin-positive phagosomes

We wanted to understand the mechanism behind F-actin recruitment to phagosomes during CR-mediated phagocytosis. The prominent deformation of sRBCs during F-actin flashes in phagosomes, and varying flashing kinetics on particles of different stiffness, prompted us to investigate whether these were a result of the mechanosensing properties of focal adhesions. CR3 is an integrin and integrins are the core of focal adhesion structures that transduce
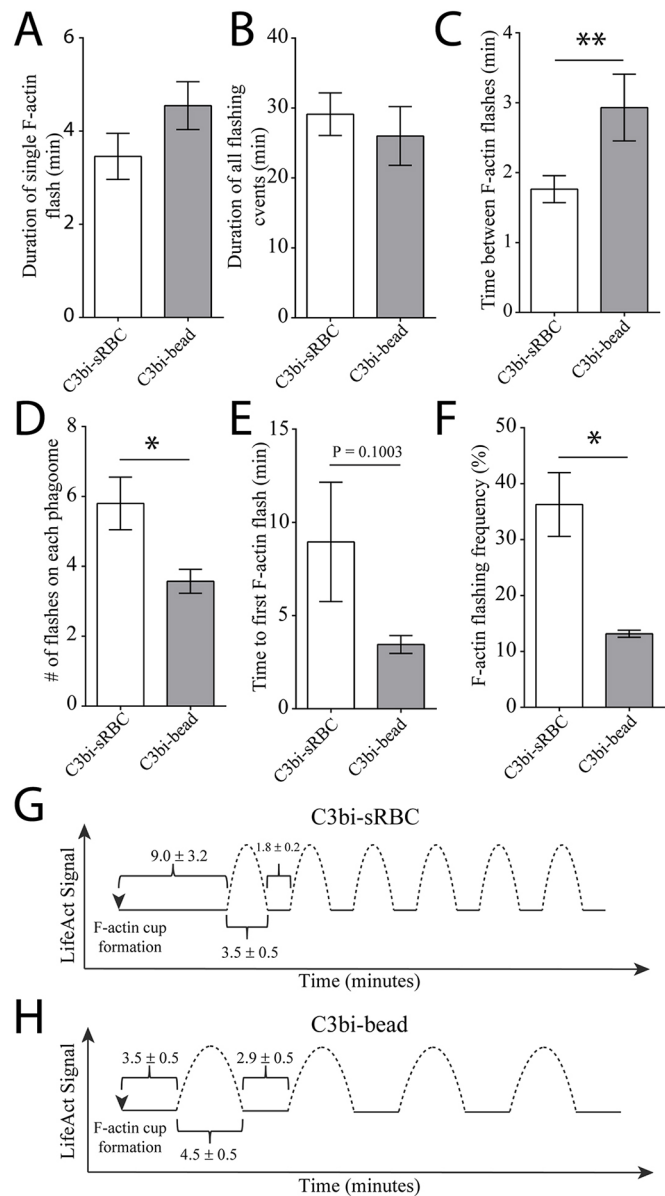
Fig. 2. Particle rigidity influences F-actin flashing dynamics on phagosomes. RAW 264.7 macrophages stably transfected with LifeAct-RFP or LifeAct-CFP were challenged with either C3bi-opsonized sRBC or C3bi-opsonized polystyrene beads (3.87 µm) and monitored with epifluorescence. (A) Duration of F-actin recruitment on phagosomes from the initial increase in LifeAct signal, back to cytosolic levels (*n*=87 F-actin flashes from C3bi-sRBC phagosomes, *n*=50 F-actin flashes from C3bi-beads phagosomes). (B) Sum of the time taken for all F-actin recruitment events on a given CR-phagosome (*n*=15 C3bi-sRBC phagosomes, *n*=14 C3bi-beads phagosomes). (C) Time interval between two F-actin flashes on a given CR-phagosome (*n*=72 intervals from C3bi-sRBC phagosomes, *n*=36 from C3bi-beads phagosomes). (D) Time for first F-actin flash on phagosomes from phagocytic cup formation (*n*=15 phagosomes for each treatment). (E) Total number of F-actin flashes on a given CR-phagosome (*n*=15 phagosomes for each treatment). (F) Frequency of F-actin flashes on CR-phagosomes (*n*=3, averages within a given field of view at 40× magnification, from a total of 67 flashing CR-phagosomes and 204 non-flashing CR-phagosomes). (G,H) Representation of F-actin flashing dynamics on C3bi-sRBCs (G) and C3bi-beads (H). Error bars represent s.e.m. **P*<0.05, ***P*<0.01.

extracellular mechanical cues to the actin cytoskeleton (Gardel et al., 2010). We first probed F-actin-positive phagosomes for CR3 and saw marked enrichment around phalloidin-positive

phagosomes at 45 min after particle internalization (Fig. 3A). Phalloidin staining for endogenous F-actin along phagosomes confirmed that F-actin flashes were not an artifact of LifeAct expression (Fig. 3A). We quantified the number of CR3-positive phagosomes for both F-actin-positive and F-actin-negative phagosomes at early (20 min) and late (45 min) times of internalization (Fig. 3B). Although most phagosomes showed detectable levels of CR3, the presence of strong CR3 immunolabeling on the phagosomes corresponded with F-actin recruitment at both time points (Fig. 3B). A small population of phalloidin-negative phagosomes enriched in CR3 was also observed (Fig. 3B). We next investigated talin, which acts as an interface between integrins and the actin cytoskeleton, and promotes integrin clustering and activation (Calderwood and Ginsberg, 2003; Janoštiak et al., 2014). Using immunofluorescence, we imaged RAW 264.7 macrophages after ingesting particles and saw strong talin enrichment around F-actin-positive phagosomes, but not on F-actin-negative phagosomes (Fig. 3A,B). To investigate the dynamics of talin recruitment to F-actin flashing phagosomes, we transfected mEmerald-talin into RAW 264.7 cells stably expressing LifeAct-RFP and performed live-cell confocal imaging during

C3bi-phagocytosis. The pattern and timing of mEmerald-talin recruitment strongly overlapped with LifeAct-RFP accumulation on phagosomes (Fig. 3C; Movie 2). We quantified the effects of this coincident recruitment on the dynamics of F-actin flashes and found that the presence of mEmerald-talin did not influence the duration of flashes on phagosomes (Fig. 3D) but did induce an extended delay between F-actin flashes compared with cells expressing LifeAct-RFP alone (Fig. 3E). To look at downstream effectors, we also probed phagosomes for total and active focal adhesion kinase (FAK, Tyr397) using immunofluorescence and found that both showed strong recruitment around F-actin-positive phagosomes exclusively (Fig. 3A,B).

Actin comet tails have been described on CR-phagosomes and are generated by phosphatidylinositol 4,5-bisphosphate [$PI(4,5)P_2$] synthesis, which in turn is thought to drive the polymerization of actin on the membrane (Bohdanowicz et al., 2010). To investigate whether $PI(4,5)P_2$ was present on flashing phagosomes, we utilized a GFP-C1-PLCδ-PH construct as a probe to monitor $PI(4,5)P_2$ activity (Stauffer et al., 1998). RAW 264.7 cells stably transfected with LifeAct-RFP were transiently transfected with GFP-C1-PLCδ-PH by electroporation. Live-cell epifluorescence imaging was
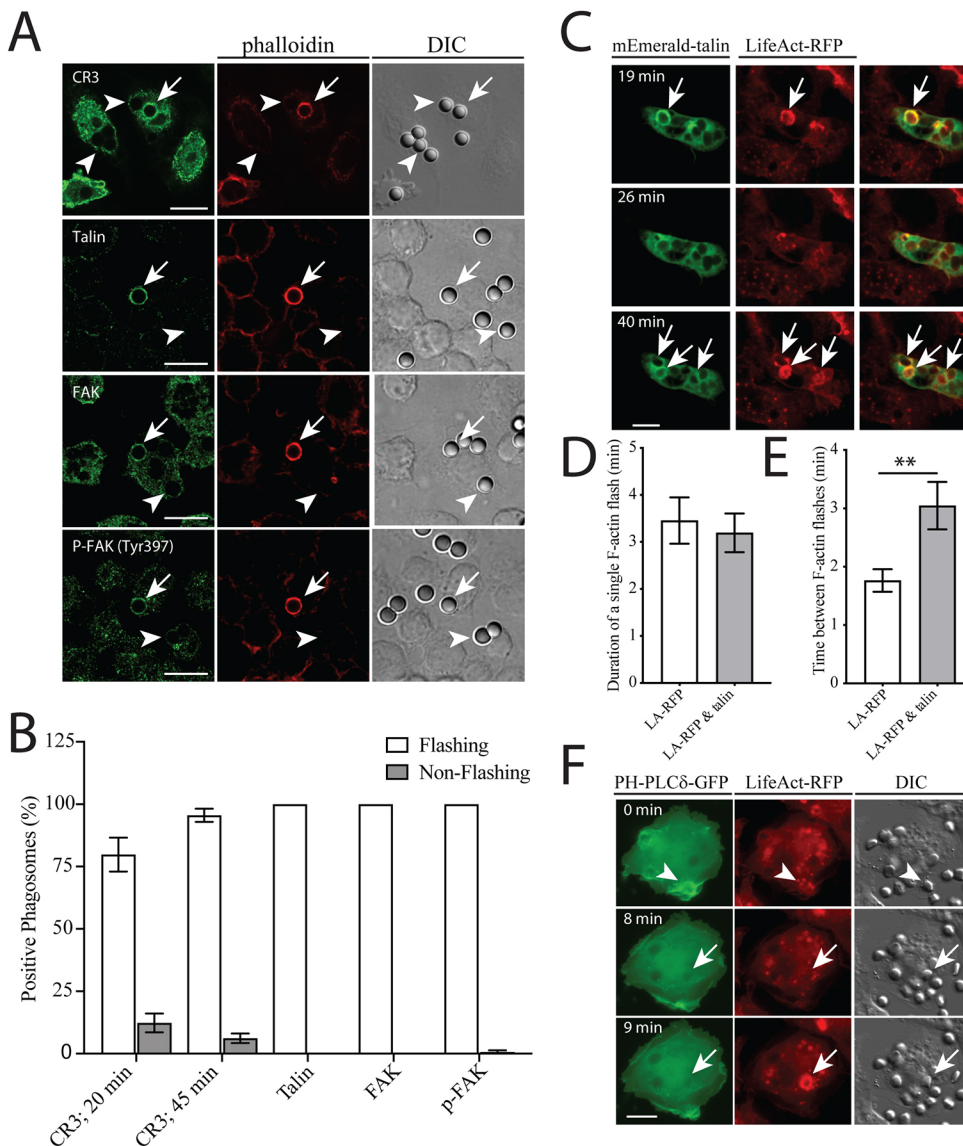

Fig. 3. CR3 integrin and focal adhesion proteins are recruited to F-actin flashes on phagosomes. (A) Immunofluorescence images of fixed RAW 264.7 macrophages challenged with C3bi-opsonized beads for 45 min. External particles were immunostained prior to cell permeabilization. F-actin was labeled with rhodamine phalloidin and cells were immunostained for CR3, talin, FAK or phospho-FAK (Tyr397). Arrows indicate F-actin flashing phagosomes and arrowheads indicate non-flashing phagosomes. (B) Quantification of recruitment of CR3, talin, FAK and phospho-FAK to flashing or non-flashing phagosomes after 45 min of internalization. CR3 recruitment to phagosomes was also analyzed at 20 min post-internalization. Numbers of phagosomes quantified were as follows: talin, n=50; FAK and phospho-FAK, n=90; CR3, n>150. (C) Live imaging of RAW 264.7 cells co-transfected with mEmerald-talin and LifeAct-RFP. Arrows indicate flashing phagosomes and time is indicated in minutes from the start of imaging. (D,E) Quantification of LifeAct (LA)-RFP flashing dynamics on 15 phagosomes from four independent movies. In mEmerald-talin transfected cells, the duration of LA-RFP recruitment to phagosomes was similar (D), but there was a significant increase in time between flashes on phagosomes, compared with cells transfected with LA-RFP alone (E). (F) Representative live-cell fluorescence images of RAW 264.7 cells stably transfected with LifeAct-RFP and transiently transfected with PH-PLCδ-GFP. Time is indicated in minutes, beginning from phagocytic cup formation. Arrowhead indicates a F-actin cup and arrows indicate a flashing phagosome that did not recruit the $PI(4,5)P_2$ probe. Error bars represent s.e.m. **P<0.01. Scale bars: 10 µm.

performed for 1 h post-C3bi-sRBC-binding with 15 s intervals between images. Although we observed an increase in GFP-C1-PLCδ-PH signal at the site of C3bi-sRBC entry, subsequent imaging of flashing and non-flashing phagosomes revealed no significant enrichment of PI(4,5)P$_2$ on phagosome membranes (Fig. 3F). Similar results were observed with the tandem PH probe (GFP-C1-PLCδ-2PH; data not shown).

RhoA effectors and Arp2/3 are recruited to F-actin-phagosomes and are required for flashing dynamics

We next investigated whether RhoA was present on flashing phagosomes. RhoA is crucial in CR-mediated phagocytosis where it influences both actin assembly and myosin II activity (Caron and Hall, 1998; Colucci-Guyon et al., 2005; Olazabal et al., 2002; Wiedemann et al., 2006). We found that RhoA immunostaining was enriched on phalloidin-positive phagosomes, but not on phalloidin-negative phagosomes (Fig. 4A,B). To determine whether the phagosome-associated RhoA was active, we exploited a RhoA biosensor in which the GBD domain of rhotekin is fused to GFP (GFP-rGBD) (Benink and Bement, 2005). RAW 264.7 cells stably expressing LifeAct-RFP were co-transfected with GFP-rGBD and imaged with spinning disk confocal microscopy during uptake of C3bi-sRBCs. The timing of enrichment of GFP-rGBD was near-simultaneous with LifeAct-RFP recruitment to phagosomes in the image snapshots acquired (Fig. 4C; Movie 3). Expression of the RhoA biosensor did not markedly influence F-actin flashing dynamics on phagosomes as the length of individual flashes was similar (Fig. 4D), with a small but insignificant increase in the time between flashes (Fig. 4E) compared with LifeAct-RFP-transfected cells alone. To understand more fully how active RhoA was being removed from phagosomes, we probed phagosomes for the RhoA-inactivating protein, p190RhoGAP (also known as ARHGAP5) (Amin et al., 2016; Ridley et al., 1993). Immunofluorescence analysis revealed that F-actin-positive but not F-actin-negative phagosomes were strongly labeled for p190RhoGAP (Fig. 4A,B).

We next tested for the functional requirement of the RhoA signaling pathway. We used a commercially available inhibitor of ROCK1, which is a downstream signaling protein of RhoA known to influence actomyosin contractility (Janoštiak et al., 2014). RAW 264.7 cells were pretreated with 10 µM of Y-27632 before being challenged with C3bi-opsonized target particles for 30 min prior to fixation and immunostaining for external particles and phalloidin to label F-actin flashes on phagosomes. In fixed cells, the overall frequency of F-actin flashing on phagosomes was intrinsically lower than in live cells, probably because of the transient nature of flashes on phagosomes (Fig. 4F). Regardless, treatment of cells with Y-27632 significantly decreased the frequency of F-actin flashes on phagosomes by ∼4.4-fold (Fig. 4F).

To investigate actin remodeling proteins, we probed for the presence of Arp2/3, as well as the Arp2/3-binding protein Wiskott–Aldrich syndrome protein (WASP), on ingested phagosomes in RAW 264.7 cells. We used an antibody to p34 (also known as ARPC2), a subunit of Arp2/3, and saw strong enrichment of both p34 and WASP on phalloidin-positive phagosomes, which was absent on non-flashing phagosomes (Fig. 4A,B). To delve more deeply into the role of Arp2/3 in F-actin flashing on phagosomes, we utilized the commercially available inhibitor CK-666, which we added to RAW 264.7 cells expressing LifeAct-RFP 15 min after particle uptake. After 45 min of particle ingestion, cells were fixed and imaged. Significantly fewer LifeAct-RFP-positive phagosomes were observed in CK-666-treated cells compared with DMSO-treated cells (Fig. 4H). We next examined the small subset of

flashing phagosomes that persisted during CK-666 treatment to understand the role of Arp2/3 in flashing dynamics and particle deformation. We performed live-cell spinning disk confocal microscopy of LifeAct-RFP-transfected cells during CR-mediated phagocytosis and CK-666 treatment. The change in F-actin flashing dynamics on phagosomes in the presence of the inhibitor was striking. Frequently, LifeAct-RFP was recruited to phagosomes in a single flash that persisted for over 10 min on average (Fig. 4G,I; Movie 4), with many protracted flashes lasting over 20 min, compared with ∼3 min in untreated cells (Fig. 2A). The average time between flashes was also higher, averaging 6 min (Fig. 4I) compared with ∼2 min in untreated cells (Fig. 2C). These two flashing phenotypes predominated in CK-666-treated macrophages (Fig. 4J). We also investigated the impact of Arp2/3 inhibition on sRBC deformation using DIC imaging. In the presence of CK-666, sRBC deformation was only observed in ∼30% of LifeAct-RFP-positive phagosomes (Fig. 4K), compared with ∼60% of flashing phagosomes in untreated cells (Fig. 1H). Thus, Arp2/3 activity is important both for F-actin flashing dynamics on phagosomes and for cargo manipulation.

Non-muscle myosin IIA is recruited to flashing phagosomes and required for phagosome content deformation

Because of the mechanical changes observed in flashing phagosome content, we next investigated whether the non-muscle myosin IIA (NMIIA) was present and important for these contractions. NMIIA is a myosin isoform found exclusively in hematopoietic cells (Maupin et al., 1994) and is required for formation of the phagocytic cup during CR-mediated phagocytosis (Olazabal et al., 2002). Using immunofluorescence, strong recruitment of NMIIA to F-actin-positive phagosomes in macrophages was observed during CR-mediated phagocytosis (Fig. 5A). To confirm the role of myosin in C3bi-sRBC deformation during F-actin flashing, we inhibited the activity of myosin IIA through blebbistatin treatment. Blebbistatin has a high affinity for the myosin-ADP-Pi complex, preventing it from releasing a phosphate group, effectively disabling it from inducing actomyosin contractions without altering its actin-binding properties (Kovács et al., 2004). We examined the effect of blebbistatin on F-actin flashing and C3bi-sRBC deformation in RAW 264.7 cells stably transfected with LifeAct-RFP (Fig. 5B). The frequency of F-actin flashes on phagosomes was slightly, but not significantly, reduced by blebbistatin treatment (Fig. 5C). We monitored sRBC deformation using DIC microscopy. The term 'deformation' was inclusive of sRBC lysis, fission and non-lytic deformation. In untreated cells, F-actin flashing phagosomes displayed deformation of sRBCs in 98.9±1.1% of cases. This was significantly reduced to 67.6±4.9% of phagosomes following blebbistatin treatment (Fig. 5D).

F-actin flashes on phagosomes delay maturation

Phagosomes fuse with both early and late endosomes and ultimately lysosomes to form phagolysosomes (Fairn and Grinstein, 2012). To detect whether F-actin flashes on phagosomes influence fusion with components of the early endocytic pathway, we immunostained cells during phagocytosis for early endosome antigen 1 (EEA1) (Steele-Mortimer et al., 1999). Spinning disk confocal microscopy imaging revealed delayed recruitment of EEA1 to phalloidin-positive phagosomes (Fig. 6A). During the first 10 min after internalization, flashing phagosomes had significantly less EEA1 recruitment than non-flashing phagosomes (Fig. 6B). At 10 min after C3bi-sRBC-internalization, 5.6±5.6% of phagosomes
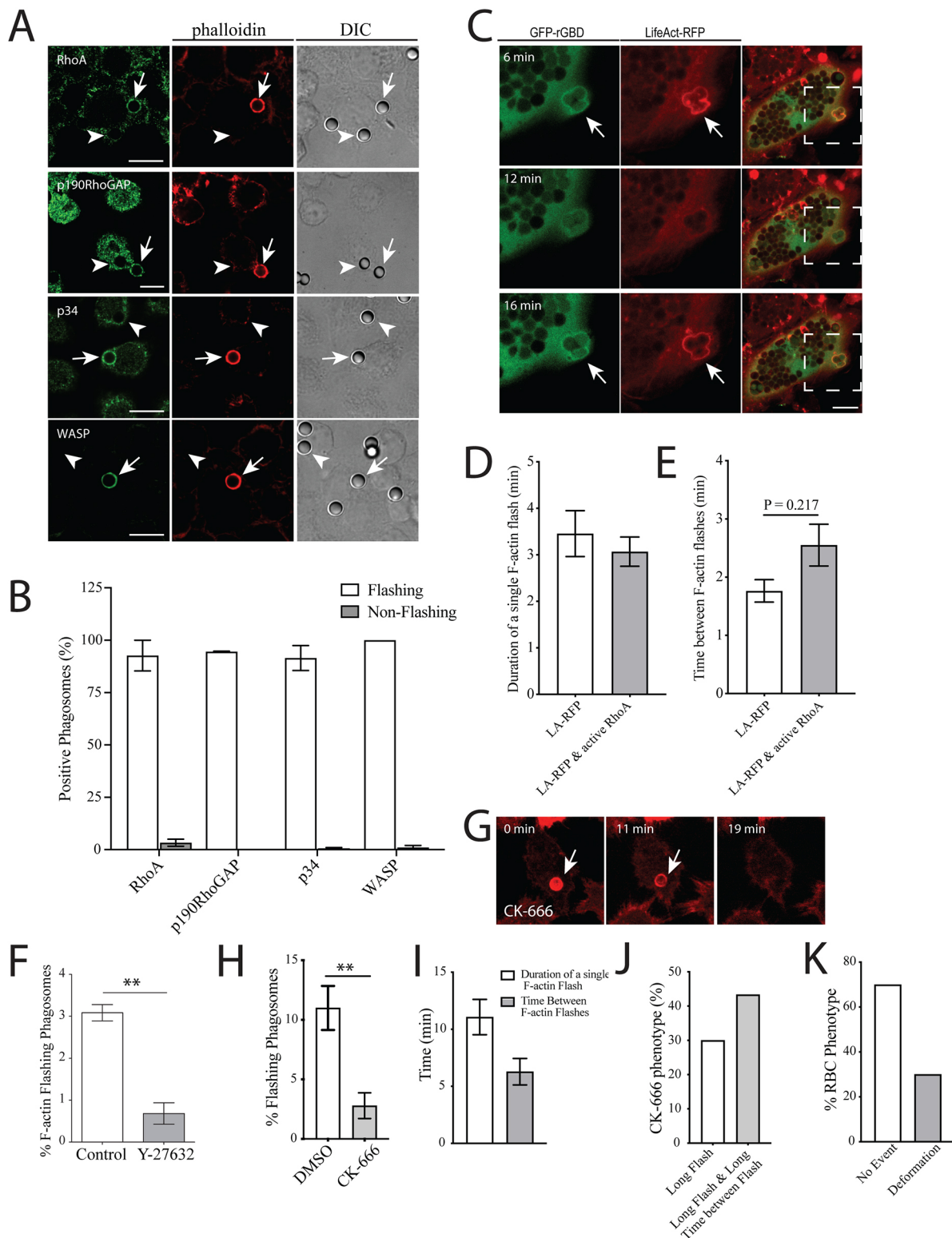
Fig. 4. See next page for legend.

enveloped with F-actin colocalized with EEA1, versus 33.1±3% of phagosomes when F-actin was absent (Fig. 6B). A delay in phagolysosome formation in FcγR-phagosomes recruiting F-actin has been previously demonstrated (Liebl and Griffiths, 2009). To investigate this during CR-mediated phagocytosis, we probed phagosomes for both F-actin and LAMP1, a marker for both

lysosomes and late endosomes (Vieira et al., 2002). The number of LAMP1-positive phagosomes (both F-actin flashing and non-flashing) was determined at 30 min after C3bi-sRBC-binding (Fig. 6C). Quantification of immunofluorescence images revealed that phagosomes without F-actin had a significantly higher frequency of LAMP1 recruitment to the membrane

Fig. 4. RhoA and Arp2/3 effectors are recruited and required for F-actin flashes on phagosomes. (A) Immunofluorescence images of fixed RAW 264.7 macrophages challenged with C3bi-opsonized beads for 45 min and stained with phalloidin for F-actin and antibodies against RhoA, p190RhoGAP, p34 Arp2/3 or WASP. Arrows indicate F-actin flashing phagosomes and arrowheads indicate non-flashing phagosomes. (B) Quantification of recruitment of RhoA, p190RhoGAP, p34 Arp2/3 or WASP to F-actin flashing or non-flashing phagosomes after 45 min of internalization. Numbers of phagosomes quantified were as follows: RhoA and WASP, n=20; p190RhoGAP, n>250; p34, n>350. (C) Live-cell imaging of RAW 264.7 cells co-transfected with GFP-rGBD and LifeAct-RFP. Arrow indicates a flashing phagosome after uptake of multiple particles and time is indicated in minutes from the start of imaging. Dashed boxes in the right-hand images indicate the region shown at higher magnification. (D,E) Quantification of GFP-rGBD flashing dynamics on seven phagosomes from four independent movies. In GFP-rGBD-transfected cells, the duration of LifeAct (LA)-RFP recruitment to phagosomes was similar (D), with a slight, but not significant, increase in time between flashes on phagosomes, compared with cells transfected with LA-RFP alone (E). (F) For ROCK inhibition, cells were pretreated with 10 µM Y-27632 ROCK inhibitor for 8 h prior to phagocytosis and fixation. F-actin was stained using rhodamine phalloidin to detect the number of flashing phagosomes in untreated cells, which was significantly reduced in Y-27632-treated cells. Three biological replicates were performed. (G) Spinning disk confocal imaging of LifeAct-RFP-expressing RAW 264.7 cells after uptake of C3bi-sRBCs and treatment with 150 µM CK-666 to inhibit Arp2/3. Arrow indicates a flashing phagosome that persisted for an extended period. Time is indicated in minutes from the start of imaging. (H) Number of phagosomes that exhibited F-actin flashes (LifeAct-RFP recruitment) in CK-666-treated cells, compared with DMSO-treated cells. (n>200 phagosomes). (I–K) Quantification of flashing dynamics and particle deformation in LifeAct-RFP-positive phagosomes in CK-666-treated macrophages; 30 flashing phagosomes from ten independent movies were analyzed. (I) Average flashing time and time between flashes in cells treated with CK-666. (J) Of the phagosomes that recruited LifeAct-RFP, frequent phenotypes included protracted (extended) flashes on phagosomes and long flashes with extended time between flashes. (K) sRBC morphology changes observed by DIC imaging in CK-666-treated cells. The majority (21/30) of sRBCs in LifeAct-RFP-positive phagosomes had no detectable change in morphology in Arp2/3-inhibited cells, with only nine out of 30 sRBCs showing detectable deformation in the presence of the drug. Error bars represent s.e.m. **P<0.01. Scale bars: 10 µm.

(87.3±2.7%) compared with F-actin-flashing phagosomes (40.3±4.8%) (Fig. 6D).

F-actin-flashing phagosomes show accelerated proteolysis at later time points

Our DIC imaging analysis revealed pronounced deformation of sRBCs in F-actin-flashing phagosomes. Correlative transmission electron microscopy (TEM) also revealed physical changes in sRBCs in phagosomes that were surrounded by a dense F-actin meshwork, compared with non-flashing phagosomes (Fig. 7A). In this assay, we identified a macrophage containing one phagosome with F-actin flashing and two phagosomes that were not flashing, using epifluorescence microscopy (Fig. 7A). TEM analysis of the macrophage showed an extensive cytoskeletal network devoid of organelles surrounding the F-actin-flashing phagosome (Fig. 7A). The magnitude of the F-actin network surrounding the phagosome has been proposed to preclude association with endocytic organelles (Liebl and Griffiths, 2009). Interestingly, the C3bi-sRBC within the F-actin-positive phagosome was much more electron dense than the sRBCs in the non-flashing phagosomes (Fig. 7A), indicating a potential compaction or rupturing of the sRBC contents.

We determined that F-actin flashes delayed phagosome maturation; however, it remains to be determined whether these pre-contractions later aid the degradation of phagosome cargo. We hypothesized that deformation of particles leading to fragmentation would increase the surface area of the phagosome contents. This
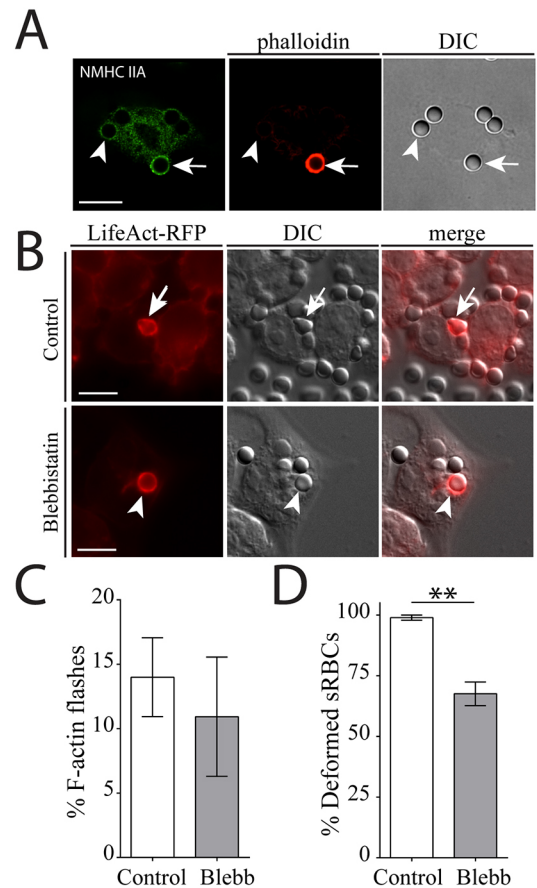
Fig. 5. Non-muscle myosin IIA is present on flashing phagosomes and its inhibition attenuates particle deformation in phagosomes. (A) Immunofluorescence images of fixed RAW macrophages challenged with C3bi-beads for a 10 min pulse, followed by washing and allowing phagocytosis to proceed for 30 min. External beads were stained with Cy5. F-actin was labeled with rhodamine phalloidin and NMIIA was immunostained with a polyclonal antibody (Biolegend). Arrows indicate a F-actin flashing phagosome that was positive for NMIIA, and arrowheads indicate a non-flashing phagosome that did not recruit myosin. (B) To test for myosin involvement in F-actin flashing and particle deformation, cells were pretreated, or not, with 100 µM blebbistatin prior to C3bi-sRBC ingestion and live fluorescent imaging. Arrows indicate a LifeAct-RFP-positive phagosome in control (DMSO) cells where particle deformation was observed using DIC imaging. Arrowheads indicate a LifeAct-RFP-positive phagosome in blebbistatin-treated cells, where no visible changes in sRBC morphology were observed by DIC microscopy. (C) Frequency of F-actin flashes for phagosomes in untreated cells compared with treated cells. (D) Frequency of phagosome deformation observed through DIC in F-actin-positive phagosomes (n>50 phagosomes from three replicates of each treatment). Error bars represent s.e.m. **P<0.01. Scale bars: 10 µm.

would augment the efficiency of degradation by proteolytic enzymes after lysosome fusion. To address this, we employed a proteolysis assay that allowed us to bind a self-quenching dye (DQ Green BSA) to C3bi-sRBCs through carbodiimide crosslinks. DQ-BSA only fluoresces after proteolysis. We fed LifeAct-RFP-expressing RAW 264.7 cells with DQ-C3bi-sRBCs and monitored DQ fluorescence up to 60 min post phagocytic cup formation (Fig. 7B). After about 30 min, DQ Green BSA fluorescence became significantly higher (~3.4-fold) in F-actin-flashing phagosomes (Fig. 7B,C), suggesting acute degradation. It remained higher than in non-flashing phagosomes until the end of the assay (60 min), when the signal was ~6.5-fold greater in F-actin-flashing phagosomes than in non-flashing phagosomes (Fig. 7C).
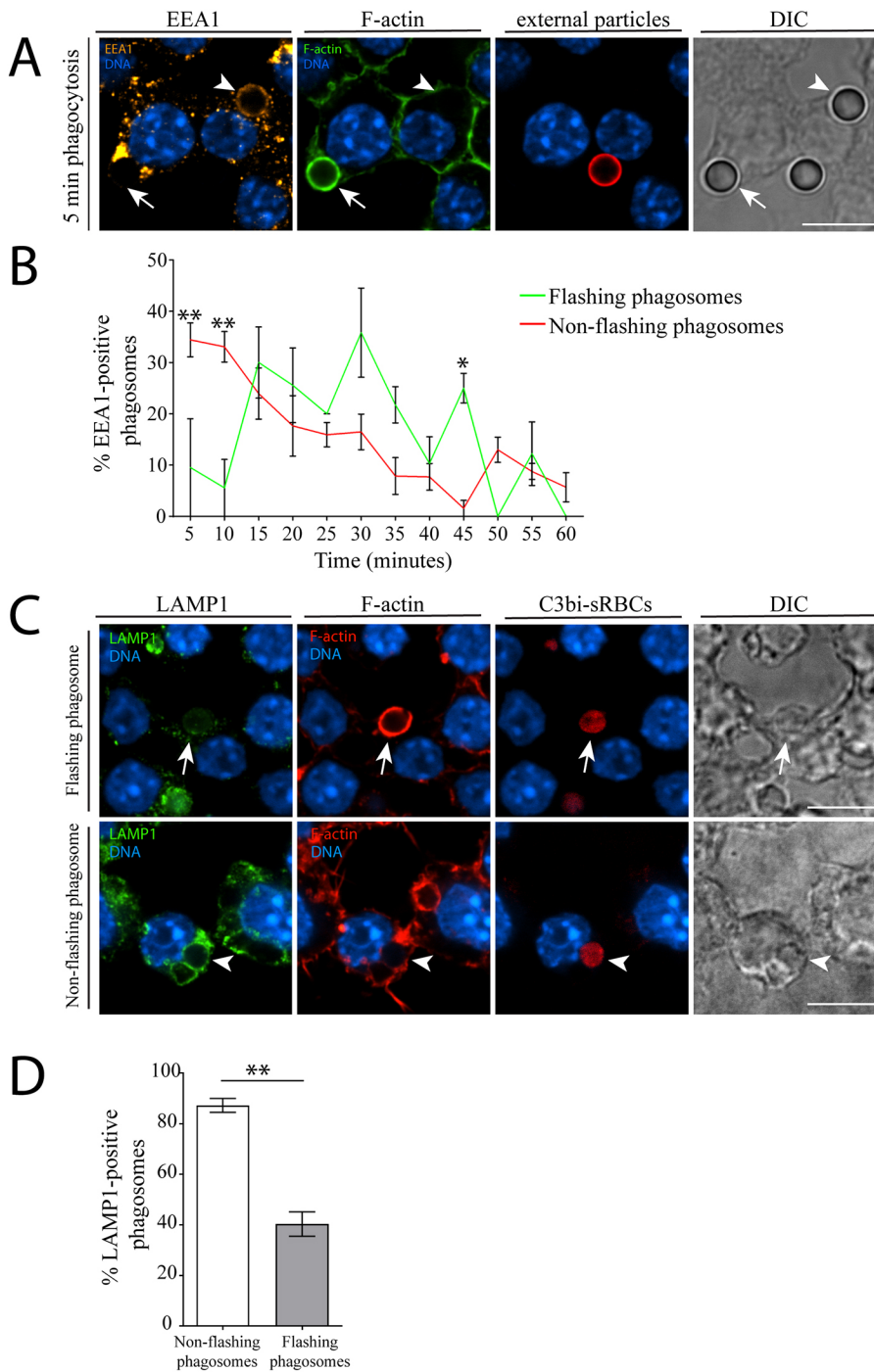
Fig. 6. F-actin flashes delay EEA1 recruitment and reduces LAMP accumulation on phagosomes. (A) RAW 264.7 cells challenged with C3bi-beads were fixed every 5 min after particle internalization for a total of 60 min and stained for EEA1 and F-actin. Arrows indicate a flashing phagosome and arrowheads indicate a phalloidin-negative phagosome. (B) EEA1 recruitment frequency to CR-phagosomes was determined at every time point (n=229 F-actin flashing CR-phagosomes across three biological replicates; n=1259 phalloidin-negative CR-phagosomes across three biological replicates). (C) To analyze the effects of F-actin flashing on phagolysosome formation, RAW 264.7 cells were fixed after 30 min of phagocytosis of C3bi-sRBCs. Cells were stained for LAMP1, F-actin and sRBCs. Arrows and arrowheads indicate flashing and non-flashing phagosomes, respectively. (D) The frequency of LAMP1-positive phagosomes was determined (n=24 flashing CR-phagosomes across three biological replicates; n=173 non-flashing phagosomes across three biological replicates). Error bars represent s.e.m. *P<0.05, **P<0.01. Scale bars: 10 μm.

DISCUSSION

This study uncovers a novel tactic within the antimicrobial arsenal employed by macrophages, involving mechanical crushing of ingested opsonized particles. This is achieved by cyclical F-actin flashes on phagosomes prior to maturation. Unlike actin comet tails previously observed on IgG- and CR-phagosomes (Bohdanowicz et al., 2010; Liebl and Griffiths, 2009), F-actin flashes do not result in translocation of the phagosome within the cytoplasm and instead appear to be responsive to phagosome content stiffness. This behavior is reminiscent of the process behind durotaxis, whereby focal adhesion turnover is mediated by substrate rigidity (Lo et al., 2000; Pelham and Wang, 1997). Migrating cells experience greater focal adhesion turnover if adhered to a soft substrate, probably a result of increased FAK activity (Plotnikov and Waterman, 2013; Schober et al., 2007). This is in line with our observation that phagosomes containing malleable cargo experience twice as many F-actin flashes than phagosomes containing latex beads.

We determined that F-actin flashes on phagosomes predominately occur on C3bi-opsonized cargo. This implicates the CR3 integrin in initiating F-actin flashes on phagosomes and, indeed, CR3 is enriched on F-actin flashing phagosomes. A small subpopulation of CR-positive and phalloidin-negative phagosomes was also identified, which might represent phagosomes in-between F-actin flashes. Ideally, we would like to investigate the activation status of CR3 on phagosomes; however, the only available antibody for detecting high affinity CR3, the CBRM1/5 monoclonal
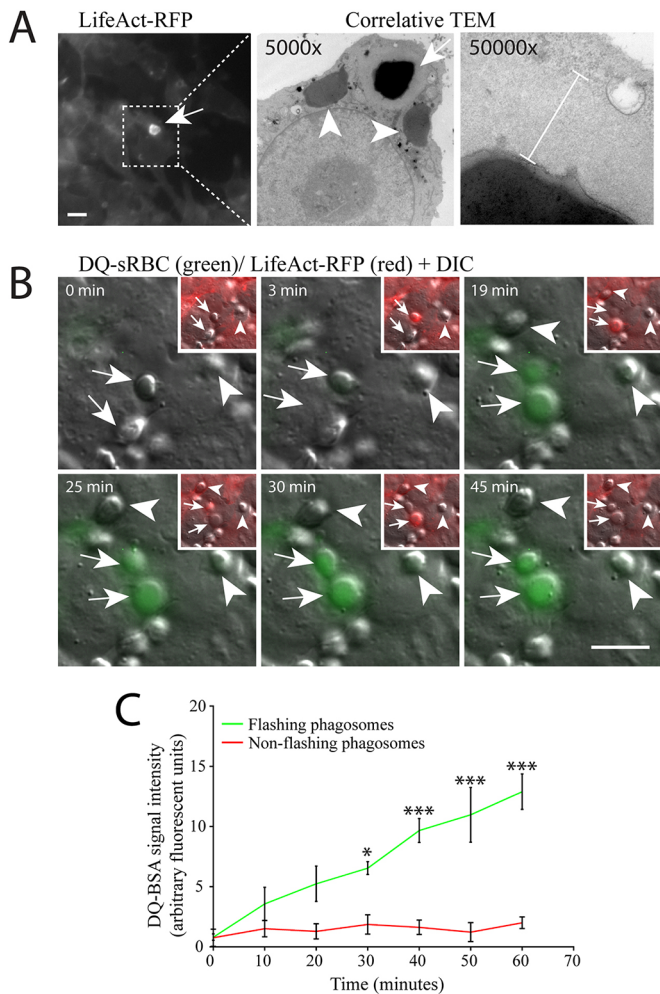
Fig. 7. F-actin flashes on phagosomes causes ultrastructural changes and enhanced degradation of internalized contents. (A) Correlative TEM analysis showing a LifeAct-CFP-positive phagosome by epifluorescence. TEM images show the same RAW 264.7 macrophage at high resolution. One phagosome is surrounded by a thick network of cytoskeleton and the sRBC is more electron dense (arrows) compared with adjacent non-flashing phagosomes (arrowheads). (B) RAW 264.7 cells stably transfected with LifeAct-RFP were challenged with DQ Green BSA-bound C3bi-sRBCs. Proteolysis of phagosome contents caused an increase in fluorescence signal intensity. Live-cell images were taken using epifluorescence microscopy, with 0 min reflecting the start of imaging. Arrows denote F-actin flashing phagosomes and arrowheads indicate non-flashing phagosomes. (C) Densitometry of DQ Green BSA signal over time in flashing and non-flashing phagosomes post phagocytic cup formation ($n=3$ biological replicates). Error bars represent s.e.m. *$P<0.05$, ***$P<0.001$. Scale bars: 10 µm.

antibody, is specific to the human protein and occludes the ligand-binding site (Diamond and Springer, 1993). The enrichment of talin on the flashing phagosome subset suggests that integrins are selectively engaged when phagosomes are flashing. Talin, a crucial link between integrins and actin filaments, promotes integrin clustering and activation by directly binding to the β-tail of integrins (Calderwood et al., 1999; Ratnikov et al., 2005). Importantly, talin is enriched at sites of C3bi-particle binding and required for internalization (Allen and Aderem, 1996; Jaumouillé et al., 2019; Lim et al., 2007). Using live-cell imaging, we observed a cyclical recruitment of mEmerald-talin coincident with LifeAct-RFP accumulation on phagosomes, indicating that talin is probably a major upstream driver of F-actin polymerization on phagosomes.

Interestingly, we observed that overexpression of talin increased the time interval between F-actin flashes, possibly as a result of cytosolic sequestration of downstream signaling elements required for F-actin flash reassembly on phagosomes. The relatively small population of flashing phagosomes that we observed during FcγR-mediated phagocytosis could be induced by a smaller, yet significant, recruitment of CR receptors to the phagosome, known to assist with FcγR-mediated phagocytosis (Jongstra-Bilen et al., 2003).

We hypothesized that cyclical recurrences of F-actin networks on phagosomes are rooted in signaling pathways typically associated with focal adhesion signal transduction. The presence of mechanosensitive focal adhesion components and an actomyosin network at the phagosome membrane could allow tension to be applied to the CR-phagosome in a controlled manner. FAK binds directly to talin (Chen et al., 1995), is responsive to mechanical forces (Seko et al., 1999), and is interestingly an essential component for CR-mediated phagocytosis in neutrophils (Kasorn et al., 2009). Curiously, we did not detect the phosphoinositide PI(4,5)P$_2$, a known activator of FAK (Cai et al., 2008), on the membrane of F-actin-positive CR-phagosomes. However, reducing FAK levels promotes RhoA activation (Ren et al., 2000). Therefore, the absence of PI(4,5)P$_2$ on phagosomes would support an increase in RhoA activity during waves of F-actin recruitment, and may indeed be a factor in the continuous polymerization of actin after phagocytic cup formation. F-actin flashes on phagosomes were enriched in RhoA, which is activated in part by the β$_2$ tail of CR3 (Wiedemann et al., 2006) and is necessary for CR-mediated phagocytosis (Caron and Hall, 1998). RhoA signaling also drives the actomyosin pulses (Munjal et al., 2015) in epithelial cells during morphogenesis (Martin et al., 2009; Rauzi et al., 2010). The actomyosin waves in epithelial cells during development are very similar, although slightly quicker in duration than those seen on phagosomes (∼100 versus 210 s on phagosomes containing C3bi-sRBCs), suggesting that similar mechanisms may be at play. RhoA GAP/GEF temporal activities set the cycles of actomyosin assembly and disassembly during the actomyosin pulses in epithelial cells (Mason et al., 2016). In agreement, the RhoA biosensor, GFP-rGBD, revealed cyclical patterns of recruitment that coincided with F-actin enrichment on flashing phagosomes. Active RhoA was not observed on non-flashing phagosomes, suggesting targeted and localized RhoA activation on flashing phagosomes. The cyclical nature of RhoA activity and its removal from the phagosome could be explained, in part, by the presence of p190RhoGAP on flashing phagosomes. Interestingly, active RhoA inactivates myosin phosphatase through ROCK, thereby promoting myosin-based contractions (Kimura et al., 1996). We saw reduced F-actin recruitment to phagosomes following ROCK inhibition, probably due to the upstream role of ROCK in activating myosin II (Amano et al., 1996).

The oscillatory nature of F-actin flashes on phagosomes is probably a combination of positive and negative feedback loops influencing F-actin dynamics. Inhibition of Arp2/3 activity decreased the prevalence of F-actin flashes on phagosomes, similar to the inhibitory effect of F-actin coating on fusing insulin granules (Ma et al., 2020). Where F-actin flashes persisted in the presence of CK-666, the flashes were abnormally long with slower turnover cycles on phagosomes. This could be caused by the drug freezing previously assembled branched actin in place on phagosomes, or a switch to formin-based F-actin polymerization, which has been reported (Henson et al., 2015; Yang et al., 2012). Within these unusual flashing phagosomes, the physical manipulation of cargo was reduced. Under normal circumstances,

F-actin depolymerization from the phagosome might occur from negative feedback loops induced by tension changes across the membrane. Tension changes modulate the binding of cofilin to F-actin (Hayakawa et al., 2011), potentially disassembling F-actin on the phagosome. RhoA activity downregulation might also be triggered by a build-up of focal adhesion components along the phagosome (Ren et al., 2000), preventing further actin polymerization. Once disassembled, repeated cycles of F-actin assembly could be a result of slip bonds between C3bi, integrin $\alpha_M\beta_2$ and talin, shown to exist for integrin binding to ECM (Jiang et al., 2003). The tension generated by F-actin flashes on phagosomes is cyclical, which would enhance the strength of the bond. In an analogous scenario, repeated application of force on fibronectin-$\alpha_5\beta_1$ bonds prolongs their lifespans in a phenomenon termed cyclical mechanical reinforcement (Kong et al., 2013). Stronger links could be produced in phagosomes containing malleable cargo. This would explain the relatively high number of F-actin flashes we observed on phagosomes containing sRBCs, to promote 'mastication' of the cargo. With malleable cargo, deformation of the substrate could lead to disengagement of integrins and reattachment to new ligands as the particle is manipulated in space. The ultimate cessation of F-actin flashing on phagosomes is probably a result of phagosome membrane remodeling that removes the crucial concentration of integrins or talin driving the signal, which remains to be tested experimentally.

In F-actin-flashing phagosomes, we noticed a delay in phagolysosome maturation, as evidenced by reduced LAMP1 staining on phalloidin-positive phagosomes. This is similar to observations in IgG-particle-overloaded macrophages, but opposite to what was seen in phagosomes associated with F-actin comet tails, which exhibited enhanced phagosome association with degradative organelles (Bohdanowicz et al., 2010; Liebl and Griffiths, 2009). It is not surprising that the presence of a dense F-actin coat precludes association with lysosomes, a strategy utilized by some internalized bacteria that recruit 'actin cages' to promote their growth (Lerm et al., 2006; Meresse et al., 2001). F-actin flashes on phagosomes strongly correlated with deformation of the ingested particles. The resulting pressure exerted from the actomyosin contractions on phagosomes was powerful enough to induce lysis of sRBCs in phagosomes. F-actin flashes on phagosomes could be analogous to chewing prior to digestion (in this case, phagosome maturation). It is also tempting to speculate that early manipulation also results in fragments of the larger particle becoming available to the macrophage to sample for antigen presentation. Indeed, we were able to capture fission events happening in concert with F-actin flashes, possibly representing an intracellular version of trogocytosis (Ahmed et al., 2008). Vesicles containing mechanically disrupted fragments would contain antigens within their native confirmation, necessary for cross-presentation (Batista and Harwood, 2009). After content sampling, the remaining 'chewed' particles, although initially experiencing a delay in maturation, would later be digested more efficiently with enzymes as a result of the increase in exposed surface area resulting from the mechanical forces.

Our discovery of F-actin flashes on phagosomes reveals a unique strategy employed by macrophages to destroy unwanted materials. Enzymatic degradation of contents within phagolysosomes is the dogma for clearance of unwanted extracellular contents and our work has added a mechanical 'chewing' activity imposed on phagosome cargo for digestion. The mastication of phagosome contents may also represent a unique strategy for obtaining native peptides from phagosomes for antigen presentation.

MATERIALS AND METHODS
Reagents and antibodies
Dulbecco's modified Eagle's medium (DMEM) and fetal bovine serum (FBS) were purchased from Wisent (St-Bruno, QC). RBC lysis buffer and macrophage colony-stimulating factor (M-CSF) were purchased from Millipore Sigma (Oakville, ON). Sheep red blood cells (sRBCs) and rabbit anti-sRBC IgG were obtained from MP Biomedical (Solon, OH); rabbit anti-sRBC immunoglobulin M (IgM) was from Cedarlane Labs (Burlington, ON). The 3.87 µm crosslinked polystyrene divinylbenzene beads P(S/2% DVB) were purchased from Bangs Laboratories (Fishers, IN). *E. coli* strain MG1655 was from the University of Toronto Scarborough teaching laboratories. Paraformaldehyde (PFA) was from Canemco & Marivac (Lakefield, QC). Rat anti-mouse CD11b antibody (M1/70) and Alexa Fluor rhodamine phalloidin were purchased from ThermoFisher Scientific (Waltham, MA). Rabbit polyclonal *E. coli* antibody was from Novus Biologicals (Centennial, CO). Mouse monoclonal anti-RhoA (26C4), mouse monoclonal anti-FAK (D-1), rabbit polyclonal anti-phospho-FAK (Tyr397), mouse monoclonal anti-RhoGAP p190-B antibody (G-11), mouse monoclonal anti-WASP (B-9), rat monoclonal anti-LAMP1 (1D4B) and goat polyclonal anti-EEA1 (N-19) antibodies were all purchased from Santa Cruz Biotechnology (Dallas, TX). Rabbit polyclonal anti-p34-Arc/ARPC2 antibody was purchased from EMD Millipore Canada Ltd (Etobicoke, ON). Rabbit polyclonal anti-non-muscle myosin heavy chain II-A antibody (Poly19098) was purchased from BioLegend (San Diego, CA). Mouse monoclonal anti-talin antibody (8d4) was purchased from Millipore Sigma. Fluorescent secondary antibodies were purchased from Jackson ImmunoResearch Laboratories (West Grove, PA). CK-666, blebbistatin, ROCK inhibitor (Y-27632), DAPI, phorbol 12-myristate 13-acetate (PMA), mouse serum, C5-deficient serum and all other reagents were purchased from Millipore Sigma (Oakville, ON).

Cell culture and transfection
The RAW 264.7 mouse macrophage cell line (TIB-71) was purchased from American Type Culture Collection (Manassas, VA). The cells were grown in DMEM containing 10% heat-inactivated FBS. RAW 264.7 macrophages (5×10^5) were plated on 35 mm dishes 2 days prior to phagocytosis assays. Primary bone marrow-derived macrophages (BMDMs) were obtained by bone marrow extraction from the femurs and tibias of male and female C57BL/6 mice [aged 3 months, in accordance with the Canadian Council on Animal Care (CCAC)], as described (Khandani et al., 2007). Transfection of macrophages was carried out using FuGENE HD (Promega; Madison, WI) in 35 mm glass-bottom dishes, as recommended by the manufacturer. Electroporation-based transfection of BMDMs were performed with a Neon transfection system (Thermo Fisher Scientific, Waltham, MA), following the manufacturer's instructions. RAW 264.7 macrophages stably transfected with LifeAct-CFP (cerulean) constructs were a gift from Dr Ray Truant (McMaster University, Hamilton, ON) and those stably transfected with LifeAct-RFP constructs were produced in the laboratory by Dr He Song Sun. The GFP-C1-PLCδ-PH construct was deposited by Tobias Meyer (Addgene plasmid # 21179) and the GFP-C1-PLCδ-2PH construct was a gift from Sergio Grinstein (Hospital for Sick Children, Toronto, ON). Plasmids also obtained from Addgene were mEmerald-talin (plasmid #54266) and GFP-rhotekin GBD (rGBD) (plasmid # 26732) (Benink and Bement, 2005).

Phagocytosis assays
sRBCs (100 µl of a 10% suspension) were washed with PBS and then opsonized with 2 mg/ml rabbit anti-sheep IgG or IgM for 1 h on a rotator at room temperature. IgM-opsonized sRBCs were washed with PBS++ (0.5 mM CaCl2 and MgCl2) and then incubated with C5-deficient human serum, as described (Jongstra-Bilen et al., 2003). Polystyrene beads were washed with PBS and opsonized with human serum IgM (2 mg/ml; Millipore Sigma) prior to C5-deficient serum treatment. Overnight cultures of *E. coli* were opsonized with 100 µl of mouse serum for 1 h at 37°C. RAW 264.7 macrophages or BMDMs were plated 2 days prior to phagocytosis assays onto glass-bottom dishes or coverslips and the complement receptors activated using 150 nM PMA in serum-free DMEM for 7 min prior to

incubation with opsonized sRBCs. Phagocytosis was allowed to proceed for specified times for live imaging, immunofluorescence or TEM analysis. For bacteria ingestion experiments, bacteria were added to cell cultures and spun onto cells at 300 g for 5 min at 8°C. For immunofluorescence assays, cells underwent phagocytosis for 15 min prior to washing of unbound particles or bacteria, after which phagocytosis was allowed to proceed for the indicated time periods. For ROCK inhibition, cells were pretreated with 10 µM Y-27632 ROCK inhibitor for 8 h prior to phagocytosis and fixation. To inhibit myosin, cells were pretreated with 100 µM blebbistatin prior to live-cell imaging. Drugs were maintained in culture during the phagocytosis assays.

Immunofluorescence
Following phagocytosis for the indicated time periods, any remaining external sRBCs were lysed with ddH$_2$O prior to fixation. Cells were fixed using 4% PFA for 20 min. C3bi-beads were used instead of C3bi-sRBCs to determine the signaling elements involved in F-actin flashes, as the human IgM bead opsonin did not overlap with the primary antibodies used. Prior to permeabilization, any external polystyrene beads were labeled with anti-human secondary antibodies. Cells were permeabilized with 0.25% Triton X-100 for 20 min prior to blocking with 10% bovine serum albumin (BSA). Primary antibody staining in 1% BSA for 1 h included anti-*E. coli* (1:200), anti-CR3 (1:100; with milk block), anti-talin (1:250), anti-FAK (1:500), anti-phospho-FAK (Tyr397) (1:500), anti-RhoA (1:150), anti-RhoGAP p190-B (1:100), anti-WASP (B-9) (1:500), anti-p34-Arc/ARPC2 (1:500), anti-non-muscle myosin heavy chain IIA (1:250), anti-EEA1 (1:250) and rat monoclonal anti-LAMP1 (1:250). After washing, cells were incubated with phalloidin (1:500) and AffiniPure Cy2 secondary antibodies (1:500), followed by DAPI staining and mounting. Images were acquired using a Quorum WaveFX-X1 spinning disk confocal system (Quorum Technologies, Guelph, ON) through MetaMorph image acquisition software (Molecular Devices, Sunnyvale, CA).

Live-cell imaging
LifeAct-CFP or LifeAct-RFP stably transfected RAW 264.7 macrophages were plated 2 days prior to imaging in 35 mm glass-bottom dishes (5×10^5 cells per dish). Serum starvation and opsonization with sRBCs or polystyrene beads were carried out according to the cell culture protocol described earlier. RAW 264.7 macrophages were activated with 150 nM PMA in serum-free DMEM 7 min prior to being challenged with 50 µl of IgG- or C3bi-sRBCs. Throughout the duration of each live imaging session, the cells were kept at 37°C and 5% CO$_2$. The objectives used included a 40× lens (oil immersion) for cell population imaging and a 63× lens (oil immersion) for single-cell imaging. Four positions were defined per 35 mm glass-bottom dish, with 15 s intervals between rounds of imaging. Live-cell imaging was conducted using a Zeiss AxioObserver Z1 (Carl Zeiss Canada, Toronto, ON) inverted epifluorescence microscope using AxioVision (version 4.9.1.0, 64 bit) software for image capture. Differential interference contrast (DIC) images were taken in addition to epifluorescence channels. On average, 240 images were taken over the course of an hour at each position on cell culture dishes. In addition, RAW 264.7 macrophages stably expressing LifeAct-RFP were transfected with mEmerald-talin or GFP-rGBD, or treated with CK-666, and imaged using a Quorum WaveFX-X1 spinning disk confocal system (Quorum Technologies, Guelph, ON) and MetaMorph image acquisition software (Molecular Devices, Sunnyvale, CA). Four to six positions were acquired at 45 s intervals for 45 min using a 63× objective lens. All other parameters were reproduced from the movies acquired with the AxioObserver Z1.

Correlative transmission electron microscopy
To look at the ultrastructure of F-actin accumulation on C3bi-sRBC-containing phagosomes, 2×10^5 RAW 264.7 macrophages stably transfected with LifeAct-RFP were plated in 6-well plates 2 days before the phagocytosis assay. The opsonization protocol for C3bi-sRBCs, as well as the live-cell epifluorescence imaging protocols described earlier, was used before sample processing for TEM. During this period of live-cell imaging, phagosomes showing F-actin recruitment were monitored before being fixed with 2% glutaraldehyde containing 0.5% saponin and 1% tannic acid for 1 h. The cells were then washed three times with 0.1 M sodium

cacodylate buffer before adding 1% osmium tetroxide and 1.25% potassium ferrocyanide in sodium cacodylate buffer and incubating for 1.5 h. The samples were washed three times with 0.1 M sodium cacodylate buffer, followed by two washes with ddH$_2$O. The samples were then stained with 4% uranyl acetate for 30 min. Prior to dehydration, the samples were washed twice with ddH$_2$O. Dehydration was achieved using ethanol ranging from 70% to 100%. For the infiltration step, a 1:1 mixture of Epon and ethanol was applied for 45 min, followed by two incubations with 100% Epon for 75 and 105 min. To embed the samples, the coverslip was inverted into a silicone mold containing Epon, which was then left overnight at 70°C. Thin sections (80 nm) were cut using a microtome before being placed on a layer of Formvar film. Finally, the processed samples were stained with uranyl acetate and lead citrate. Images were acquired with a Hitachi H7500 TEM (Hitachi High Technologies Canada, Rexdale, ON).

Proteolysis assay
To measure the intensity of proteolysis in phagosomes, an adaptation of a protocol developed by the Botelho research group was followed (Kim et al., 2014). sRBCs (200 µl) were re-suspended in 500 µL 1× PBS and 25 mg/ml of carbodiimide crosslinker. The mixture was placed on a rotator for 15 min. Excess carbodiimide was washed off three times with 1 ml of PBS (centrifugation at 3000 g for 5 min). The sRBC pellet was then re-suspended in 500 µl of PBS containing 1 mg of DQ Green BSA (conjugated with BODIPY FL fluorophores) (Thermo Fisher Scientific, Waltham, MA). The mixture was left on a rotator at 4°C for 12 h, while being protected from light. Excess DQ Green BSA was washed off three times with 500 ml of PBS (centrifugation at 3000 g for 5 min). The final pellet was re-suspended in around 200 µl of PBS and opsonized with C3bi using the same protocol as previously described. RAW 264.7 macrophages were challenged with DQ-C3bi-sRBCs and imaged using epifluorescence microscopy under the same parameters as previously described for live-cell imaging. Quantification for the proteolysis assay was based on densitometry measurements over 60 min. Three flashing and non-flashing phagosomes were monitored for DQ fluorescence. Images from the green channel (DQ Green BSA) at each time point were converted to grayscale using Adobe Photoshop CS6 (Adobe Systems, San Jose, CA). Densitometry measurements were taken using ImageJ (version 1.48, 64 bit; NIH, Bethesda, MD). Mean background density was subtracted from the mean density of the phagosome lumen for both flashing and non-flashing phagosomes. The average density value of the three flashing and non-flashing phagosomes was taken before each value was normalized to the initial value at time 0. The resulting numbers represented the fold-change in DQ Green BSA intensity from the initial measurements.

Image analysis, quantifications and statistical tests
Images acquired by epifluorescence microscopy were quantified using AxioVision (version 4.9.1.0, 64 bit; Carl Zeiss Canada) and ImageJ (version 1.48, 64 bit; NIH, Bethesda, MD). Spinning disk confocal image acquisition was carried out using MetaMorph; image processing was done using Volocity for fixed cell analyses (contrast adjustments and file exportation). Spinning disk confocal movies were acquired using MetaMorph and processed using Fiji/ImageJ (version 2.0) with the plugins Bio-Formats, Z Projection and Annotation to Overlay. TEM images were acquired, processed and exported using iTEM (version 5.2; Olympus Soft Imaging Solutions, Muenster, Germany). Figures were prepared using Adobe Illustrator CS6 (Adobe Systems, San Jose, CA).

For quantification purposes, F-actin flashing during live-cell phagocytosis was defined as brief and symmetrical increases in F-actin polymerization at the phagosome membrane, occurring post phagocytic cup formation. The F-actin flashes observed using DIC imaging were characteristically transient and oscillatory (more than one round of F-actin recruitment) in stationary phagosomes that were often associated with target particle deformation. To quantify F-actin flash dynamics and intensity, an region of interest (ROI) was defined around an internalized particle from image frames acquired using live epifluorescence microscopy that was then processed using Volocity (version 6.1.1, 64 bit; Perkin Elmer, Waltham, MA). Quantification of frames began when the C3bi-sRBC became bound to the macrophage. The arbitrary fluorescence intensity unit (AFU) from

the appropriate color channel was taken for every frame in the defined ROI. The frequency of F-actin flashing on phagosomes was calculated by dividing the number of flashing phagosomes by the total number of phagosomes.

Unless otherwise indicated, for quantifications, 50 phagosomes were assayed in three biological replicates. For the immunofluorescence assays, F-actin-positive and F-actin-negative phagosomes were scored for enrichment of candidate proteins. Total phagosomes assayed were RhoA and WASP (20 phagosomes), talin (50 phagosomes), FAK and phospho-FAK (Tyr397) (90 phagosomes), CR3 (>150 phagosomes for each time point), p190RhoGAP (>250 phagosomes) and p34 (>350 phagosomes). EEA1-positive phagosomes were tabulated at 5 min intervals post-internalization. The percentage of EEA1-positive phagosomes among total phagosomes over time (1 h) was then calculated. The number of LAMP1-positive phagosomes was determined for both F-actin flashing and non-flashing phagosomes to calculate and compare the proportion of LAMP1-positive phagosomes in both cases. Three independent experiments were performed for these assays.

For Arp2/3 inhibition assays, phagocytosis was performed for 15 min to ensure particle internalization prior to addition of 150 µM CK-666. LifeAct-RFP-transfected cells were then imaged live; DMSO- and CK-666-treated cells were left for an additional 30 min prior to fixation. For ROCK inhibition assays, the percentage of phalloidin-positive phagosomes for each condition (treated and untreated) was determined by counting phagosomes using the 'Cell Counter' plug-in for ImageJ (version 1.48, 64 bit; NIH, Bethesda, MD). Three independent experiments were conducted. Live-cell DIC imaging was used to assess qualitatively the deformation of C3bi-sRBCs through visual inspection in blebbistatin-treated cells. A C3bi-sRBC was considered deformed if its circularity was noticeably altered (≥10% change by eye) and occurred synchronously with F-actin flashing. Slight fluid-like motions on the surface of phagosome membranes during F-actin flashes were not sufficient to be considered noticeable alterations of C3bi-sRBC circularity. Cells were imaged every 30 s for 2 h, at multiple positions on the glass coverslips. Deformation frequency (deformed C3bi-sRBCs divided by non-deformed C3bi-sRBCs) was compared between flashing and non-flashing phagosomes. The frequency of C3bi-sRBC deformation phenotypes was calculated by dividing the number of flashing phagosomes exhibiting one of the three phenotypes by the total number of flashing CR-phagosomes.

An unpaired two-tailed Student's *t*-test was used to determine statistical significance between two groups (*P*-value <0.05 was considered statistically significant). For comparing three groups or more, a non-parametric one-way ANOVA was used, followed by Tukey's test for multiple comparisons. The mean±s.e.m. of each group is displayed in both cases. Prism (version 5.0) was used to conduct the statistical analyses (GraphPad Software, La Jolla, CA).

Peer review history
The peer review history is available online at
https://jcs.biologists.org/lookup/doi/10.1242/jcs.239384.reviewer-comments.pdf

References
Ahmed, K. A., Munegowda, M. A., Xie, Y. and Xiang, J. (2008). Intercellular trogocytosis plays an important role in modulation of immune responses. *Cell. Mol. Immunol.* **5**, 261-269. doi:10.1038/cmi.2008.32

Allen, L. A. and Aderem, A. (1996). Molecular definition of distinct cytoskeletal structures involved in complement- and Fc receptor-mediated phagocytosis in macrophages. *J. Exp. Med.* **184**, 627-637. doi:10.1084/jem.184.2.627

Amano, M., Ito, M., Kimura, K., Fukata, Y., Chihara, K., Nakano, T., Matsuura, Y. and Kaibuchi, K. (1996). Phosphorylation and activation of myosin by Rho-associated kinase (Rho-kinase). *J. Biol. Chem.* **271**, 20246-20249. doi:10.1074/jbc.271.34.20246

Amin, E., Jaiswal, M., Derewenda, U., Reis, K., Nouri, K., Koessmeier, K. T., Aspenstrom, P., Somlyo, A. V., Dvorsky, R. and Ahmadian, M. R. (2016). Deciphering the molecular and functional basis of RHOGAP family proteins: a systematic approach toward selective inactivation of rho family proteins. *J. Biol. Chem.* **291**, 20353-20371. doi:10.1074/jbc.M116.736967

Batista, F. D. and Harwood, N. E. (2009). The who, how and where of antigen presentation to B cells. *Nat. Rev. Immunol.* **9**, 15-27. doi:10.1038/nri2454

Benink, H. A. and Bement, W. M. (2005). Concentric zones of active RhoA and Cdc42 around single cell wounds. *J. Cell Biol.* **168**, 429-439. doi:10.1083/jcb.200411109

Bohdanowicz, M., Cosío, G., Backer, J. M. and Grinstein, S. (2010). Class I and class III phosphoinositide 3-kinases are required for actin polymerization that propels phagosomes. *J. Cell Biol.* **191**, 999-1012. doi:10.1083/jcb.201004005

Cai, X., Lietha, D., Ceccarelli, D. F., Karginov, A. V., Rajfur, Z., Jacobson, K., Hahn, K. M., Eck, M. J. and Schaller, M. D. (2008). Spatial and Temporal Regulation of Focal Adhesion Kinase Activity in Living Cells. *Mol. Cell. Biol.* **28**, 201-214. doi:10.1128/MCB.01324-07

Calderwood, D. A. and Ginsberg, M. H. (2003). Talin forges the links between integrins and actin. *Nat. Cell Biol.* **5**, 694-696. doi:10.1038/ncb0803-694

Calderwood, D. A., Zent, R., Grant, R., Rees, D. J. G., Hynes, R. O. and Ginsberg, M. H. (1999). The talin head domain binds to integrin β subunit cytoplasmic tails and regulates integrin activation. *J. Biol. Chem.* **274**, 28071-28074. doi:10.1074/jbc.274.40.28071

Caron, E. and Hall, A. (1998). Identification of two distinct mechanisms of phagocytosis controlled by different Rho GTPases. *Science* **282**, 1717-1721. doi:10.1126/science.282.5394.1717

Chen, H.-C., Appeddu, P. A., Parsons, J. T., Hildebrand, J. D., Schaller, M. D. and Guan, J. L. (1995). Interaction of focal adhesion kinase with cytoskeletal protein talin. *J. Biol. Chem.* **270**, 16995-16999. doi:10.1074/jbc.270.28.16995

Colucci-Guyon, E., Niedergang, F., Wallar, B. J., Peng, J., Alberts, A. S. and Chavrier, P. (2005). A role for mammalian diaphanous-related formins in complement receptor (CR3)-mediated phagocytosis in macrophages. *Curr. Biol.* **15**, 2007-2012. doi:10.1016/j.cub.2005.09.051

Diamond, M. S. and Springer, T. A. (1993). A subpopulation of Mac-1 (CD11b/CD18) molecules mediates neutrophil adhesion to ICAM-1 and fibrinogen. *J. Cell Biol.* **120**, 545-556. doi:10.1083/jcb.120.2.545

Fairn, G. D. and Grinstein, S. (2012). How nascent phagosomes mature to become phagolysosomes. *Trends Immunol.* **33**, 397-405. doi:10.1016/j.it.2012.03.003

Gardel, M. L., Schneider, I. C., Aratyn-Schaus, Y. and Waterman, C. M. (2010). Mechanical integration of actin and adhesion dynamics in cell migration. *Annu. Rev. Cell Dev. Biol.* **26**, 315-333. doi:10.1146/annurev.cellbio.011209.122036

Hayakawa, K., Tatsumi, H. and Sokabe, M. (2011). Actin filaments function as a tension sensor by tension-dependent binding of cofilin to the filament. *J. Cell Biol.* **195**, 721-727. doi:10.1083/jcb.201102039

Henson, J. H., Yeterian, M., Weeks, R. M., Medrano, A. E., Brown, B. L., Geist, H. L., Pais, M. D., Oldenbourg, R. and Shuster, C. B. (2015). Arp2/3 complex inhibition radically alters lamellipodial actin architecture, suspended cell shape, and the cell spreading process. *Mol. Biol. Cell* **26**, 887-900. doi:10.1091/mbc.E14-07-1244

Janoštiak, R., Pataki, A. C., Brábek, J. and Rösel, D. (2014). Mechanosensors in integrin signaling: the emerging role of p130Cas. *Eur. J. Cell Biol.* **93**, 445-454. doi:10.1016/j.ejcb.2014.07.002

Jaumouillé, V., Cartagena-Rivera, A. X. and Waterman, C. M. (2019). Coupling of β2 integrins to actin by a mechanosensitive molecular clutch drives complement receptor-mediated phagocytosis. *Nat. Cell Biol.* **21**, 1357-1369. doi:10.1038/s41556-019-0414-2

Jiang, G., Giannone, G., Critchley, D. R., Fukumoto, E. and Sheetz, M. P. (2003). Two-piconewton slip bond between fibronectin and the cytoskeleton depends on talin. *Nature* **424**, 334-337. doi:10.1038/nature01805

Jongstra-Bilen, J., Harrison, R. and Grinstein, S. (2003). Fcγ-receptors induce Mac-1 (CD11b/CD18) mobilization and accumulation in the phagocytic cup for optimal phagocytosis. *J. Biol. Chem.* **278**, 45720-45729. doi:10.1074/jbc.M303704200

Kasorn, A., Alcaide, P., Jia, Y., Subramanian, K. K., Sarraj, B., Li, Y., Loison, F., Hattori, H., Silberstein, L. E., Luscinskas, W. F. et al. (2009). Focal adhesion kinase regulates pathogen-killing capability and life span of neutrophils via mediating both adhesion-dependent and -independent cellular signals. *J. Immunol.* **183**, 1032-1043. doi:10.4049/jimmunol.0802984

Khandani, A., Eng, E., Jongstra-Bilen, J., Schreiber, A. D., Douda, D., Samavarchi-Tehrani, P. and Harrison, R. E. (2007). Microtubules regulate PI-3K activity and recruitment to the phagocytic cup during Fc gamma receptor-mediated phagocytosis in nonelicited macrophages. *J. Leukoc. Biol.* **82**, 417-428. doi:10.1189/jlb.0706469

Kim, G. H. E., Dayam, R. M., Prashar, A., Terebiznik, M. and Botelho, R. J. (2014). PIKfyve inhibition interferes with phagosome and endosome maturation in macrophages. *Traffic* **15**, 1143-1163. doi:10.1111/tra.12199

Kimura, K., Ito, M., Amano, M., Chihara, K., Fukata, Y., Nakafuku, M., Yamamori, B., Feng, J., Nakano, T., Okawa, K. et al. (1996). Regulation of myosin phosphatase by Rho and Rho-associated kinase (Rho-kinase). *Science* **273**, 245-248. doi:10.1126/science.273.5272.245

Kong, F., Li, Z., Parks, W. M., Dumbauld, D. W., García, A. J., Mould, A. P., Humphries, M. J. and Zhu, C. (2013). Cyclic mechanical reinforcement of integrin-ligand interactions. *Mol. Cell* **49**, 1060-1068. doi:10.1016/j.molcel.2013.01.015

Kovács, M., Tóth, J., Hetényi, C., Málnási-Csizmadia, A. and Sellers, J. R. (2004). Mechanism of blebbistatin inhibition of myosin II. *J. Biol. Chem.* **279**, 35557-35563. doi:10.1074/jbc.M405319200

Lerm, M., Holm, A., Seiron, A., Särndahl, E., Magnusson, K.-E. and Rasmusson, B. (2006). Leishmania donovani requires functional Cdc42 and Rac1 to prevent phagosomal maturation. *Infect. Immun.* **74**, 2613-2618. doi:10.1128/IAI.74.5.2613-2618.2006

Liebl, D. and Griffiths, G. (2009). Transient assembly of F-actin by phagosomes delays phagosome fusion with lysosomes in cargo-overloaded macrophages. *J. Cell Sci.* **122**, 2935-2945. doi:10.1242/jcs.048355

Lim, J., Wiedemann, A., Tzircotis, G., Monkley, S. J., Critchley, D. R. and Caron, E. (2007). An essential role for talin during alpha(M)beta(2)-mediated phagocytosis. *Mol. Biol. Cell* **18**, 976-985. doi:10.1091/mbc.e06-09-0813

Lo, C.-M., Wang, H.-B., Dembo, M. and Wang, Y.-l. (2000). Cell movement is guided by the rigidity of the substrate. *Biophys. J.* **79**, 144-152. doi:10.1016/S0006-3495(00)76279-5

Ma, W., Chang, J., Tong, J., Ho, U., Yau, B., Kebede, M. A. and Thorn, P. (2020). Arp2/3 nucleates F-actin coating of fusing insulin granules in pancreatic beta cells to control insulin secretion. *J. Cell Sci.* **133**, jcs236794. doi:10.1242/jcs.236794

Martin, A. C., Kaschube, M. and Wieschaus, E. F. (2009). Pulsed contractions of an actin-myosin network drive apical constriction. *Nature* **457**, 495-499. doi:10.1038/nature07522

Mason, F. M., Xie, S., Vasquez, C. G., Tworoger, M. and Martin, A. C. (2016). RhoA GTPase inhibition organizes contraction during epithelial morphogenesis. *J. Cell Biol.* **214**, 603-617. doi:10.1083/jcb.201603077

Maupin, P., Phillips, C. L., Adelstein, R. S. and Pollard, T. D. (1994). Differential localization of myosin-II isozymes in human cultured cells and blood cells. *J. Cell Sci.* **107**, 3077-3090.

Meresse, S., Unsworth, K. E., Habermann, A., Griffiths, G., Fang, F., Martinez-Lorenzo, M. J., Waterman, S. R., Gorvel, J.-P. and Holden, D. W. (2001). Remodelling of the actin cytoskeleton is essential for replication of intravacuolar Salmonella. *Cell. Microbiol.* **3**, 567-577. doi:10.1046/j.1462-5822.2001.00141.x

Munjal, A., Philippe, J.-M., Munro, E. and Lecuit, T. (2015). A self-organized biomechanical network drives shape changes during tissue morphogenesis. *Nature* **524**, 351-355. doi:10.1038/nature14603

Olazabal, I. M., Caron, E., May, R. C., Schilling, K., Knecht, D. A. and Machesky, L. M. (2002). Rho-kinase and myosin-II control phagocytic cup formation during CR, but not FcgammaR, phagocytosis. *Curr. Biol.* **12**, 1413-1418. doi:10.1016/S0960-9822(02)01069-2

Patel, P. C. and Harrison, R. E. (2008). Membrane ruffles capture C3bi-opsonized particles in activated macrophages. *Mol. Biol. Cell* **19**, 4628-4639. doi:10.1091/mbc.e08-02-0223

Pelham, R. J. and Wang, Y.-l. (1997). Cell locomotion and focal adhesions are regulated by substrate flexibility. *Proc. Natl. Acad. Sci. USA* **94**, 13661-13665. doi:10.1073/pnas.94.25.13661

Plotnikov, S. V. and Waterman, C. M. (2013). Guiding cell migration by tugging. *Curr. Opin. Cell Biol.* **25**, 619-626. doi:10.1016/j.ceb.2013.06.003

Ratnikov, B. I., Partridge, A. W. and Ginsberg, M. H. (2005). Integrin activation by talin. *J. Thromb. Haemost.* **3**, 1783-1790. doi:10.1111/j.1538-7836.2005.01362.x

Rauzi, M., Lenne, P.-F. and Lecuit, T. (2010). Planar polarized actomyosin contractile flows control epithelial junction remodelling. *Nature* **468**, 1110-1114. doi:10.1038/nature09566

Ren, X. D., Kiosses, W. B., Sieg, D. J., Otey, C. A., Schlaepfer, D. D. and Schwartz, M. A. (2000). Focal adhesion kinase suppresses Rho activity to promote focal adhesion turnover. *J. Cell Sci.* **113**, 3673-3678.

Ridley, A. J., Self, A. J., Kasmi, F., Paterson, H. F., Hall, A., Marshall, C. J. and Ellis, C. (1993). rho family GTPase activating proteins p190, bcr and rhoGAP show distinct specificities in vitro and in vivo. *EMBO J.* **12**, 5151-5160. doi:10.1002/j.1460-2075.1993.tb06210.x

Riedl, J., Crevenna, A. H., Kessenbrock, K., Yu, J. H., Neukirchen, D., Bista, M., Bradke, F., Jenne, D., Holak, T. A., Werb, Z. et al. (2008). Lifeact: a versatile marker to visualize F-actin. *Nat. Methods* **5**, 605-607. doi:10.1038/nmeth.1220

Schober, M., Raghavan, S., Nikolova, M., Polak, L., Pasolli, H. A., Beggs, H. E., Reichardt, L. F. and Fuchs, E. (2007). Focal adhesion kinase modulates tension signaling to control actin and focal adhesion dynamics. *J. Cell Biol.* **176**, 667-680. doi:10.1083/jcb.200608010

Seko, Y., Takahashi, N., Tobe, K., Kadowaki, T. and Yazaki, Y. (1999). Pulsatile stretch activates mitogen-activated protein kinase (MAPK) family members and focal adhesion kinase (p125(FAK)) in cultured rat cardiac myocytes. *Biochem. Biophys. Res. Commun.* **259**, 8-14. doi:10.1006/bbrc.1999.0720

Stauffer, T. P., Ahn, S. and Meyer, T. (1998). Receptor-induced transient reduction in plasma membrane PtdIns(4,5)P2 concentration monitored in living cells. *Curr. Biol.* **8**, 343-346. doi:10.1016/S0960-9822(98)70135-6

Steele-Mortimer, O., Meresse, S., Gorvel, J.-P., Toh, B.-H. and Finlay, B. B. (1999). Biogenesis of Salmonella typhimurium-containing vacuoles in epithelial cells involves interactions with the early endocytic pathway. *Cell. Microbiol.* **1**, 33-49. doi:10.1046/j.1462-5822.1999.00003.x

Vieira, O. V., Botelho, R. J. and Grinstein, S. (2002). Phagosome maturation: aging gracefully. *Biochem. J.* **366**, 689-704. doi:10.1042/bj20020691

Wiedemann, A., Patel, J. C., Lim, J., Tsun, A., van Kooyk, Y. and Caron, E. (2006). Two distinct cytoplasmic regions of the β2 integrin chain regulate RhoA function during phagocytosis. *J. Cell Biol.* **172**, 1069-1079. doi:10.1083/jcb.200508075

Wright, S. D. and Silverstein, S. C. (1982). Tumor-promoting phorbol esters stimulate C3b and C3b' receptor-mediated phagocytosis in cultured human monocytes. *J. Exp. Med.* **156**, 1149-1164. doi:10.1084/jem.156.4.1149

Yam, P. T. and Theriot, J. A. (2004). Repeated cycles of rapid actin assembly and disassembly on epithelial cell phagosomes. *Mol. Biol. Cell* **15**, 5647-5658. doi:10.1091/mbc.e04-06-0509

Yang, Q., Zhang, X.-F., Pollard, T. D. and Forscher, P. (2012). Arp2/3 complex-dependent actin networks constrain myosin II function in driving retrograde actin flow. *J. Cell Biol.* **197**, 939-956. doi:10.1083/jcb.201111052